Journal of Fundamental and Applied Sciences

Research Article

ISSN 1112-9867

Available online at http://www.jfas.info

CAMBRIDGE CRYSTALLOGRAPHIC DATABASE ANALYSIS OF SOME MEDICINALLY IMPORTANT HALOGENATED AMINOPYRIDINES

Ruchika Sharma[1], Saminathan Murugavel[2] and Rajni Kant[3,*]

[1]Department of Physics, University of Jammu, Jammu Tawi, 180006, Jammu & Kashmir, India

[2]Department of Physics, Thanthai Periyar Government Institute of Technology, Vellore, 632002, Tamil Nadu, India

[3]Vice-Chancellor, Rabindranath Tagore University, Post-Bhojpur, Bhopal-Chiklod Road, Raisen, 464993, Madhya Pradesh, India

Received: 13 February 2024 / Accepted: 31 March 2024 / Published: 31 March 2024

ABSTRACT

A database comparison of the crystal structure of some halogenated aminopyridine derivatives has been performed for their structural optimization and quantum chemical analysis. The investigation explores the optimum structural geometry of the identified molecules, including the frontier orbital energy gap, Mulliken atomic charge distribution and molecular electrostatic potential (MEP). The two-dimensional fingerprint plots and Hirshfeld surface analysis reveals diverse intermolecular interactions existing between the molecules. The void volume percentage has been computed to infer about the physical strength of these molecules. Molecular docking has been performed to reveal that all the molecules could be potential candidates for an efficient potent inhibitor for MET receptor.

Keywords: X-ray structure, Optimization, HOMO-LUMO, Hirshfeld surfaces, Molecular docking.

Author Correspondence, e-mail: rkant.ju@gmail.com

doi: http://dx.doi.org/10.4314/jfas.1368

1. INTRODUCTION

Halogenated aminopyridines constitute a class of compounds known for their remarkable biological properties. These compounds not only serve as crucial intermediates in the production of various derivatives with diverse applications in the field of medical science, they also exhibit effectiveness across a spectrum of drugs used for the anticancer, antiviral, anti-tuberculosis, anti-malarial, antifungal, and antidiabetic care [1-6]. Halogenated aminopyridines have become crucial contributors in the endeavor to develop impactful therapeutic interventions, especially in the treatment of cancer—a predominant global cause of mortality and suffering [7]. The activation of receptor tyrosine kinases, such as MET, has been identified as a pivotal mechanism in triggering and advancing cancer development. Consequently, extensive research has focused on the MET receptor, establishing it as a well-established therapeutic target in a variety of malignancies [8]. As of now, a number of small molecule tyrosine kinase inhibitors targeting MET, such as crizotinib, cabozantinib, capmatinib, and tepotinib, are likely to be used for the treatment of specific cancer types [9].

Besides this, certain aminopyridines contribute to the development of antibacterial drugs. Therefore, in view of the importance of aminopyridine derivatives, a series of few such chemically-similar-looking aminopyridines were mined from the Cambridge Structural Database (CSD ver. 2023) and the identified structures are : (M1) 2-amino-5-bromo-pyridine (CSD code: CAJXAN), (M2) 2-amino-5-chloropyridine (AMCLPY12), (M3) 2-amino-3-bromo-4-methylpyridine (TUHCAB), (M4) 3,5-Dibromo-6-methylpyridin-2-amine (DAWTUT) and (M5) 3,5-Dichloro-6-methylpyridin-2-amine (DOKWUW) [10-14]. Each structure has been put to an extensive theoretical crystallographic investigation using Density Functional Theory and Hirshfeld surface and the molecular docking analysis has been conducted to assess the potential of these molecules to interact with the MET receptor. Figure 1 contains the chemical structure of each molecule.

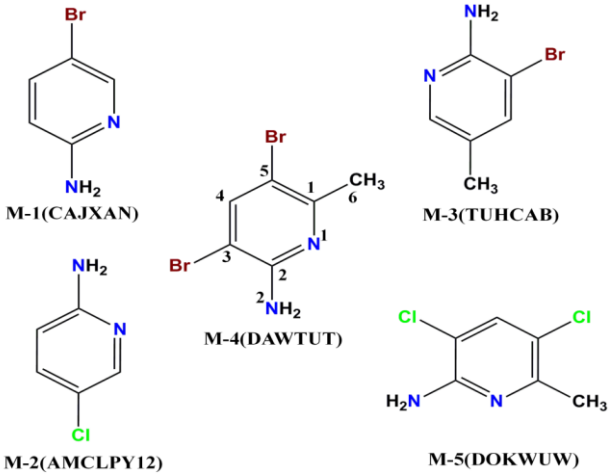

Fig.1. Chemical structures of aminopyridines structures (M1-M5) with CSD codes and atomic numbering scheme

2. COMPUTATIONAL DETAILS

2.1. Quantum chemical calculations

In view of having reported only the X-ray structure of M1 – M5, the quantum chemical investigations have been performed to have an inspection of close level of confidence between the experimental and optimized geometry of each structure. The Gaussian 09 software has been employed to conduct density functional theory (DFT), optimizing the molecular geometry of each aminopyridine derivative in the gas phase [15]. The optimized geometrical calculation is based on the B3LYP functional and basis set 6-311++G(d,p), and conceivable correlations were made between the observed and theoretically determined parameters[16-18].

2.2. Hirshfeld surface (HS) analysis

The Hirshfeld surface, serving as a visual tool, is employed to identify different intermolecular interactions within the crystal structure of a molecule and plays a crucial role in quantifying the significance of each interaction for ensuring the stability of the packing arrangement [19,20]. The Hirshfeld surfaces were generated using Crystal Explorer 21.5 [21]. The computational approach involved 3D surface and 2D fingerprint graph analysis for scrutinizing the proximity of neighboring atoms, their contact affinity and the normalized contact distance (d_{norm}), which accounts for the space between two atoms across the surface

relative to atomic radii [22,23]. This calculation is based on distances to the closest nuclei outside the surface (d_e) and within the surface (d_i), taking into consideration the van der Waals radii of atoms [24]. Moreover, the Hirshfeld surface, utilizing a (0.002 au) isosurface of the spherical promolecular electron density, aids in identifying voids within crystal structures [25]. This approach provides insights into void spaces in crystalline materials, including computed surface areas and volumes of the voids [26–28].

2.3. Molecular docking analysis

The docking analysis has been carried out against the MET receptor to explore binding modes and important molecular interactions between the molecule and the target's binding site. AutoDock Vina software was employed, utilizing the target protein with PDB ID: 3LQ8 [29, 30]. During protein structure refinement, hydrogen atoms were added while water molecules and native ligands were removed. However, the Kollmann charges were applied to the receptors. Grid coordinates (X = -0.8414, Y = 3.8741, and Z = 29.0205) were used to define the active site of the protein. These coordinates show the exact area within the protein where the compound is expected to bind. The ligand-protein interactions have been analyzed using Discovery Studio 4.1 Visualizer software [31].

3. RESULTS AND DISCUSSION

3.1. Crystallographic comparison

Table 1 presents precise crystal data for each structure, featuring a notably low reliability index (R-factor) of 2.73% for M-2 and 2.40% for M-5. This low R-factor is attributed to the collection of data for these structures at a lower temperature, enhancing the overall accuracy and reliability of the crystallographic information. All the structures crystallize in the monoclinic crystal system with Z =4, and the radiation used is Mo K_α, except for structure M-1 (Cu K_α).

Table 1. Precise X-ray crystallographic data of each structure

Parameters	M1	M2	M3	M4	M5
CCDC code	CAJXAN	AMCLPY12	TUHCAB	DAWTUT	DOKWUW

Chemical Formula	$C_5H_5Br_1N_2$	$C_5H_5ClN_2$	$C_6H_7BrN_2$	$C_6H_6Br_2N_2$	$C_6H_6Cl_2N_2$
Radiation	Cu K_α	Mo K_α	Mo K_α	Mo K_α	Mo K_α
Temperature	295 K	100(2) K	292(2) K	296(2) K	100.00(10) K
Crystal system	Monoclinic	Monoclinic	Monoclinic	Monoclinic	Monoclinic
Space group	$P2_1/c$	$P2_1/c$	$P2_1/n$	$P2_1/n$	$P2_1/n$
Unit cell volume (Å^3)	595.3(9)	540.1(3)	717.9(5)	801.54(2)	723.01(3)
Z	4	4	4	4	4
R-factor	7.90	2.73	3.41	3.81	2.40

3.2. Structure optimization

The molecular geometry of all five structures has been optimized using the DFT method, utilizing the B3LYP/6-311++G(d,p) basis set. A comparative analysis has been conducted to evaluate the concordance between the bond distances and angles derived from theoretical computations and those determined experimentally through X-ray structure analysis. The findings, presented in Table 2, indicate a positive correlation between the experimental and theoretical values, underscoring the reliability of the theoretical approach.

Table 2. Comparative bond parameters: XRD vs. DFT

Parameters	**M1 (CAJXAN)**		**M2 (AMCLPY12)**		**M3 (TUHCAB)**		**M4 (DAWTUT)**		**M5 (DOKWUW)**	
	XRD	**DFT**	**XRD**	**DFT**	**XRD**	**DFT**	**XRD**	**DFT**	**XRD**	**DFT**
BOND DISTANCE (Å)										
C1-N1	1.325	1.335	1.348	1.334	1.339	1.334	1.358	1.338	1.347	1.338
C2-N1	1.343	1.338	1.351	1.338	1.349	1.336	1.338	1.338	1.341	1.337
C2-N2	1.364	1.380	1.360	1.381	1.361	1.373	1.364	1.369	1.361	1.371
C2-C3	1.421	1.409	1.410	1.409	1.405	1.412	1.406	1.409	1.412	1.409
C3-C4	1.374	1.384	1.375	1.383	1.368	1.381	1.366	1.382	1.373	1.381

C4-C5	1.389	1.394	1.397	1.394	1.397	1.401	1.390	1.392	1.394	1.391
C5-C1	1.377	1.388	1.379	1.388	1.379	1.393	1.375	1.399	1.389	1.399
BOND ANGLE (°)										
C1-N1-C2	117.9	118.7	118.1	118.7	118.7	119.4	120.6	121.5	121.0	121.3
N1-C2-C3	121.7	122.1	121.7	122.1	119.9	120.0	120.3	120.4	120.1	120.5
C2-C3-C4	118.7	118.7	119.4	118.7	120.3	120.0	120.1	119.4	120.1	119.4
C3-C4-C5	118.4	118.6	118.5	118.6	119.9	119.8	118.2	118.7	118.2	118.5
C4-C5-C1	118.6	118.9	119.2	118.9	116.3	115.9	120.8	119.8	120.2	119.9
C5-C1-N1	123.9	122.8	122.9	122.8	124.8	124.7	120.0	120.2	120.3	120.3
N1-C1-N2	118.3	116.4	116.7	116.4	117.3	117.1	116.7	116.8	117.6	117.1
C3-C2-N1	119.9	121.4	121.5	121.4	122.8	122.8	122.9	122.8	122.3	122.3

3.3. Energy gap analysis

The HOMO-LUMO orbitals computed by the DFT/B3LYP/6-311G++(d,p) method have a significant effect on the chemical properties of molecules [32-33]. The HOMO orbitals, more frequent in all five structures, are spread out over the whole moiety, while the LUMO orbitals are mostly on the pyridine ring [34]. In general, the most stable molecules are those that have higher ΔE values. The ΔE value analysis reveals that the molecules (M1-M5) are more stable and less reactive due to their high energy gaps (Figure 2).

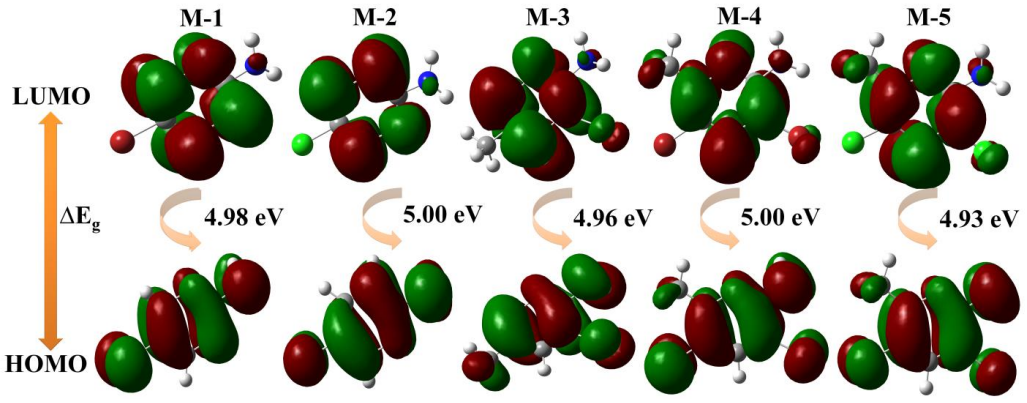

Fig.2. HOMO-LUMO energy gaps

3.4. MEP and Atomic charge analysis

The molecular electrostatic potential (MEP) and the atomic charges were calculated using the DFT method. The negative areas (pale yellow), as shown in Figure 3, are concentrated mostly around the nitrogen and bromine atoms while the positive regions (blue) are located on the amino groups. According to the Mulliken charge analysis (Table 3), all nitrogen and carbon atoms, except C3 and C5, in molecules (M1–M5) are negatively charged. The analysis of the Molecular Electrostatic Potential (MEP) and Mulliken charge distributions offers valuable insights into the presence of electrophilic and nucleophilic regions within these structures, elucidating their reactivity and capacity for chemical interactions.

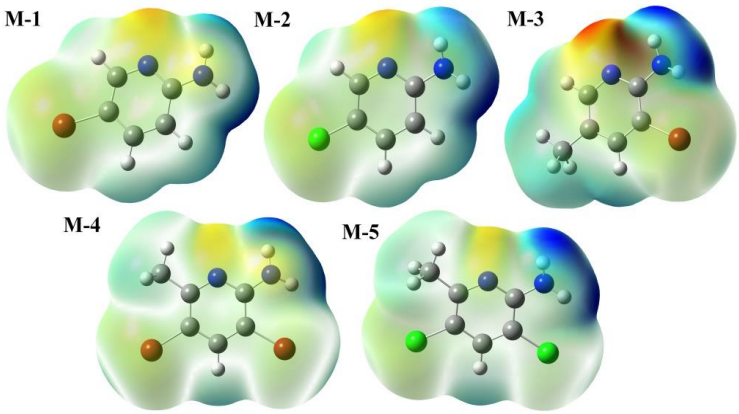

Fig.3. Molecular electrostatic maps of M1-M5

Table 3. Lists of Mulliken atomic charges of molecules M1-M5

Atoms	**M1 (CAJXAN)**	**M2 (AMCLPY12)**	**M3 (TUHCAB)**	**M4 (DAWTUT)**	**M5 (DOKWUW)**
N1	-0.118	-0.137	-0.098	-0.009	-0.022
N2	-0.263	-0.264	-0.228	-0.249	-0.247
C1	-0.247	-0.388	-0.567	-0.305	-0.809
C2	-0.561	-0.605	-0.600	-0.417	-0.279
C3	0.436	0.415	0.714	0.714	0.535
C4	-0.362	-0.685	-0.231	-0.520	-1.223
C5	0.143	0.262	0.489	0.382	0.951

3.5. Hirshfeld surfaces and Fingerprint plots

Figure 4 shows the Hirshfeld surface of M1, M2, M3, M4 and M5 contour over d_{norm}. The molecular Hirshfeld surfaces are color-coded based on the d_{norm} values, with red spots highlighting intercontacts associated with hydrogen bonds. The magnitude of these spots corresponds to the intensity or strength of the associated contacts. The bright red spots indicate the existence of N-H…N interactions in all the molecules. The visualisation of the shape-index and curvedness plots for all five structures indicates the absence of planar stacking (π-π) interactions (Figure 4). All the molecules differ significantly in their crystal packings due to vacant positions (Figure 5). The Crystal Explorer 21.5 software has been used to analyze the presence of voids in each crystal structure [21]. This analysis included the use of a procrystal electron density isosurface with a threshold of 0.002 atomic units. The void volume percentages for M1 (6.4%), M2 (3.6%), M3 (10.0%), M4 (7.5%), and M5 (6.02%) show the high physical strength of the molecule M2.

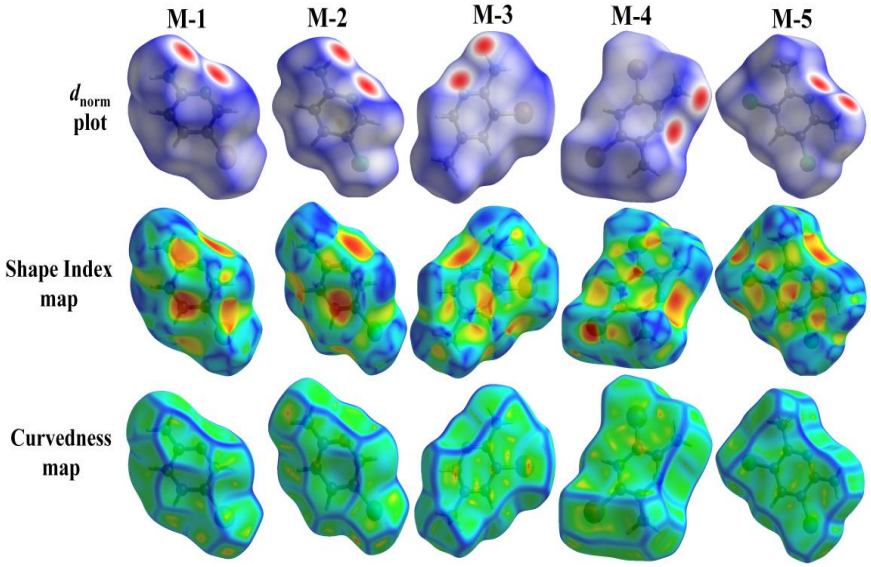

Fig.4. Hirshfeld surfaces (d_{norm}, Shape index and Curvedness) of molecules M-1 to M-5

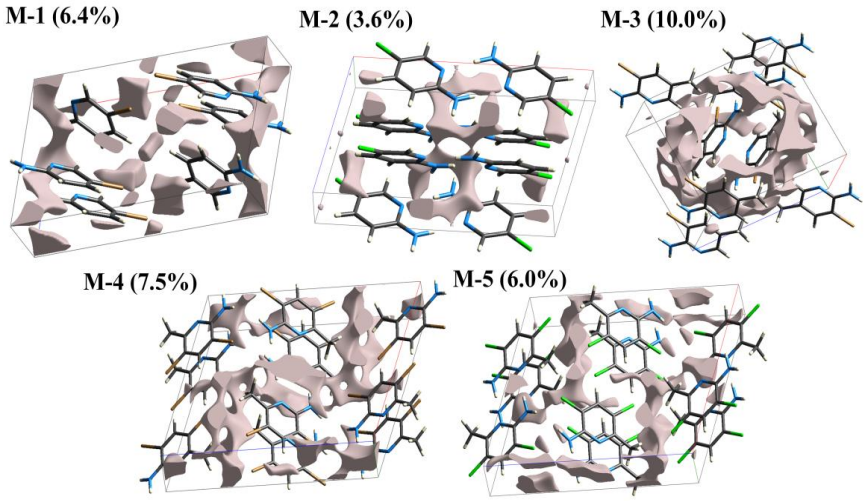

Fig.5. Crystal voids analysis of M-1 to M-5.

In Figure 6, the two-dimensional fingerprint plots are shown. These plots show how the interactions between molecules affect the overall Hirshfeld surface area [35]. In the instances of M4 and M5, the contribution of H...Br (41.1%) and H...Cl (39.4%) contacts surpasses that of the other molecules. The molecule M3 displays the highest proportion of H…H contacts, constituting 43.3% of the total contribution. There are distinct peaks in the fingerprint plots that draw attention to the prominent intermolecular contacts. The hydrogen-halogen interactions are shown by two distinct wings, playing a significant role in the molecular packing of each structure.

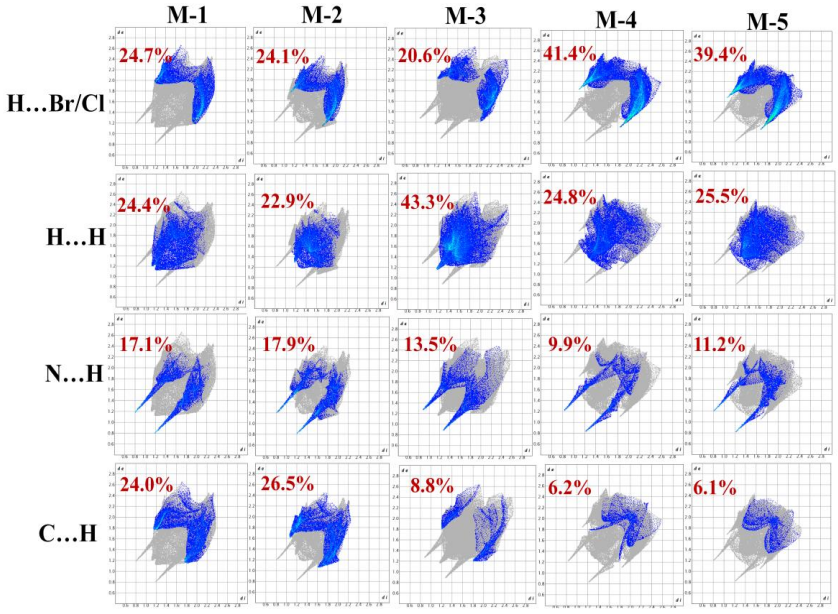

Fig.6. Two dimensional FPPs of molecules M1-M5

3.6. Molecular Docking Analysis

The binding poses of M1 - M5 and that of Cabozantinib and Crizotinib compounds at the binding site of 3LQ8 are shown in Figure 7(a-g). The two-dimensional (2D) binding interactions of these compounds with the 3LQ8 binding sites are shown in Figure 8 while the binding energy, distance, and bonding type of the compounds with 3LQ8 are presented in Table 4.

In M1–3LQ8 complex, there are several interactions which stabilize the compound, besides the conventional hydrogen bond interaction between the residue MET101and two nitrogen atoms of M1 (distances ≈ 2.585 Å and 2.216 Å), respectively, and a hydrogen bond interaction between PRO99 and compound M1 (distance = 2.699 Å). A Pi-Donor hydrogen bond exists between TYR100 and ligand at a distance of 3.302 Å. Hydrophobic interactions include Pi-Sigma bonding between the carbon atoms of the MET152 with six membered ring of ligand M1 at a distance 3.302 Å. Further, three Alkyl interactions occur between residues ILE32, LEU85 and LEU98 with bromine and carbon atoms of the ligand M1 at distances of 4.289 Å, 5.045 Å and 3.964 Å, respectively. The exists conventional hydrogen bond interaction between MET101 and nitrogen atom of compound M2 at distances of 2.686 Å, in case of M2-3LQ8 complex, while another interaction occurs between the ligand M2 donating hydrogen to PRO99 at a distance of 2.500 Å. The bromine and carbon atoms of M2 result in the formation of five Alkyl interactions with residues ALA56, ILE32, LEU85 and LEU98 and four Pi-Alkyl bonding with residues TYR100, PHE164, ALA56 and ILE32, respectively.

The M3–3LQ8 complex features conventional hydrogen bond interactions, with M3 donating two hydrogens to the residue PRO99 at a distance of 2.511 Å and 2.778 Å, respectively. The chlorine and carbon atoms of M3 form five Alkyl bonding with ALA56, ILE32, LEU85 and LEU98 and four Pi-Alkyl interactions with TYR100, PHE164, ALA56 and ILE32 residues, respectively. The residues ASP163 and PHE164 makes two conventional hydrogen bond interactions with M4-3LQ8 complex at a distance of 2.555 Å and 2.13951 Å, respectively. It makes two hydrophobic interactions including the Alkyl bonding with ALA56 and VAL40, and also forms four Pi-Alkyl interactions with PHE164, LYS58, LEU98, and ALA167, respectively. The M5–3LQ8 complex demonstrates a conventional hydrogen bond interaction

between PHE164 and M5 at a distance of 2.219 Å. There exists a hydrophobic interaction (Pi-Pi Stacked) between M5 and PHE164 protein at a distance of 4.310 Å. The bromine and carbon atoms of M5 results in the formation of three Alkyl interactions with ALA56, VAL40 and MET152 at distances of 4.462 Å, 4.736 Å and 4.781 Å and three Pi-Alkyl interactions with LEU98, LYS58 and PHE164 residues.

The Cabozantinib–3LQ8 complex stabilizes with one carbon hydrogen bond and four hydrophobic interactions including one Pi-Sigma and three Alkyl bonds. Further, the Crizotinib–3LQ8 complex also stabilizes with one hydrogen bond and four hydrophobic interactions including two Pi-Sigma and two Alkyl bonds. Comparing the number of interactions and their types, it has been observed that M2 and M3 have the highest number of interactions including both hydrogen bonds and various hydrophobic interactions, indicating a potentially strong binding to the 3LQ8 binding site. The M3–3LQ8 complex displaying a binding energy of -5.3 Kcal/mol confirms the capability of this molecule to act as an effective inhibitor against the MET receptor.

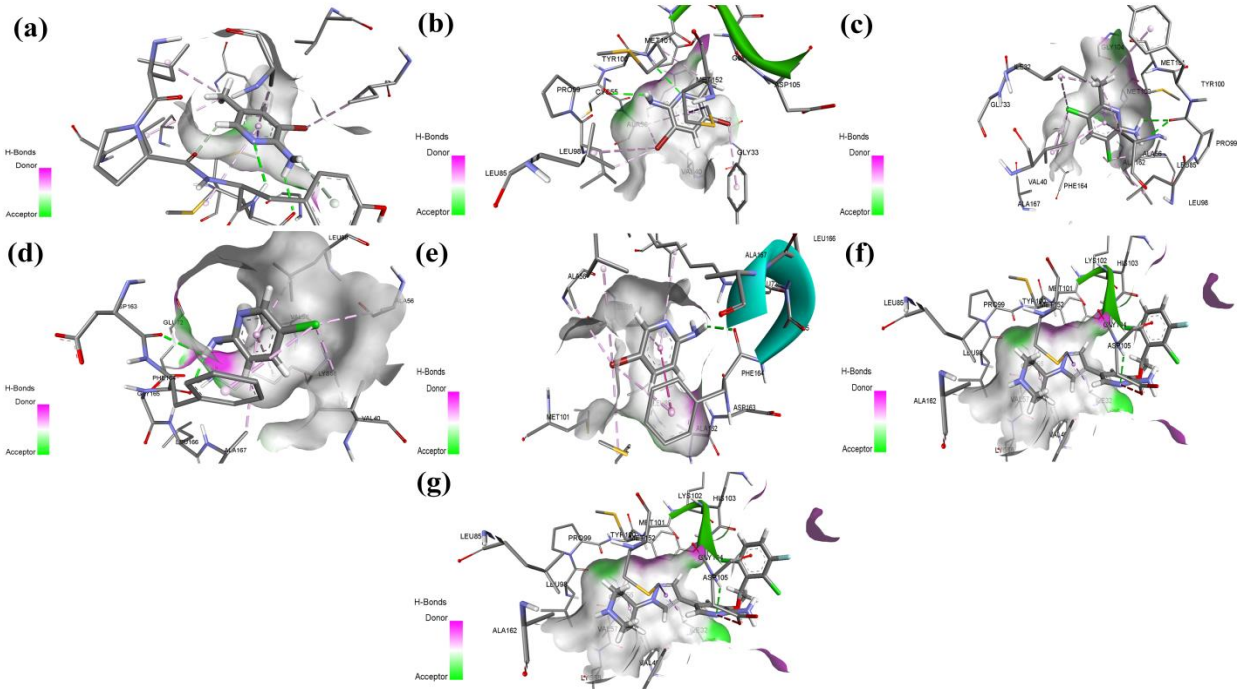

Fig.7. The binding poses of M1, M2, M3, M4, M5, Cabozantinib, and Crizotinib compounds at the binding site of 3LQ8

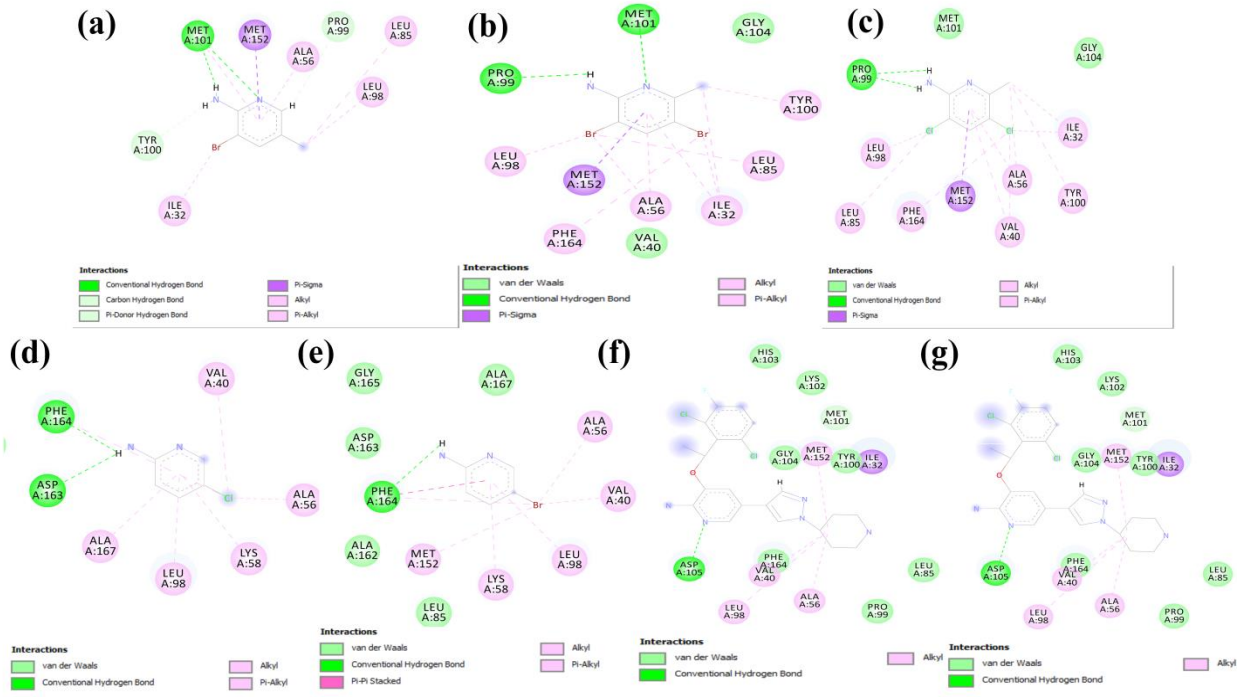

Fig.8. The 2D binding interaction of M, M2, M3, M4, M5, Cabozantinib and Crizotinib compounds at the binding site of 3LQ8 (Hydrogen atoms are omitted for clarity)

Table 4. Binding energy, Hydrogen bond, Electrostatic and Hydrophobic contacts of molecules M1-M5, Cabozantinib and Crizotinib with 3LQ8

Inhibitor	Binding Energy (Kcal mol^{-1})	Interactions	Distance (Å)	Bonding	Bonding Types
M1	- 4.9	MET101[NH….N]	2.585	Hydrogen Bond	Conventional Hydrogen Bond
		MET101[O....H]	2.216	Hydrogen Bond	Conventional Hydrogen Bond
		PRO99[O....H]	2.699	Hydrogen Bond	Carbon Hydrogen Bond
		TYR100 [π.....H]	3.302	Hydrogen Bond	Pi-Donor Hydrogen Bond

		MET152[CH..... π]	3.613	Hydrophobic	Pi-Sigma
		ILE32[π .....Br]	4.289	Hydrophobic	Alkyl
		LEU85[π .....C]	5.045	Hydrophobic	Alkyl
		LEU98[π .....C]	3.964	Hydrophobic	Alkyl
		ALA56[C.....π]	3.763	Hydrophobic	Pi-Alkyl
		MET101[C.....π]	5.169	Hydrophobic	Pi-Alkyl
M2	-5.2	MET101[NH.....N]	2.686	Hydrogen Bond	Conventional Hydrogen Bond
		PRO99[O....H]	2.500	Hydrogen Bond	Conventional Hydrogen Bond
		MET152[CH..... π]	3.414	Hydrophobic	Pi-Sigma
		ALA56 [π .....Br]	3.922	Hydrophobic	Alkyl
		ILE32[π .....Br]	4.721	Hydrophobic	Alkyl
		ILE32[π .....C]	4.511	Hydrophobic	Alkyl
		LEU85[π .....Br]	5.488	Hydrophobic	Alkyl
		LEU98[π .....Br]	4.147	Hydrophobic	Alkyl
		TYR100 [π .....C]	5.126	Hydrophobic	Pi-Alkyl
		PHE164 [π .....Br]	4.958	Hydrophobic	Pi-Alkyl
		ILE32[π .....C]	4.901	Hydrophobic	Pi-Alkyl
		ALA56[π .....C]	4.265	Hydrophobic	Pi-Alkyl
M3	-5.3	PRO99[O....H]	2.511	Hydrogen Bond	Conventional Hydrogen Bond
		PRO99[O....H]	2.778	Hydrogen Bond	Conventional Hydrogen Bond
		MET152[C.....π]	3.802	Hydrophobic	Pi-Sigma
		ALA56 [π .....C]	4.240	Hydrophobic	Alkyl
		ILE32[π .....Cl]	4.208	Hydrophobic	Alkyl
		VAL40[π .....Cl]	3.715	Hydrophobic	Alkyl

		ILE32[π .....C]	4.104	Hydrophobic	Alkyl
		LEU85[π .....Cl]	4.772	Hydrophobic	Alkyl
		LEU98[π .....Cl]	3.829	Hydrophobic	Alkyl
		TYR100 [π .....C]	5.111	Hydrophobic	Pi-Alkyl
		PHE164 [π .....Cl]	4.829	Hydrophobic	Pi-Alkyl
		VAL40[π .....C]	5.084	Hydrophobic	Pi-Alkyl
		ALA56[π .....C]	3.905	Hydrophobic	Pi-Alkyl
M4	-4.8	ASP163[O....H]	2.555	Hydrogen Bond	Conventional Hydrogen Bond
		PHE164[O....H]	2.140	Hydrogen Bond	Conventional Hydrogen Bond
		ALA56 [π .....Cl]	4.020	Hydrophobic	Alkyl
		VAL40[π .....Cl]	4.384	Hydrophobic	Alkyl
		PHE164 [π .....Cl]	5.167	Hydrophobic	Pi-Alkyl
		LYS58[C.....π]	4.662	Hydrophobic	Pi-Alkyl
		LEU98[C.....π]	4.756	Hydrophobic	Pi-Alkyl
		ALA167[C.....π]	5.256	Hydrophobic	Pi-Alkyl
M5	-4.9	PHE164[O....H]	2.219	Hydrogen Bond	Conventional Hydrogen Bond
		PHE164 [π.....π]	4.309	Hydrophobic	Pi-Pi Stacked
		ALA56 [π .....Br]	4.462	Hydrophobic	Alkyl
		VAL40[π .....Br]	4.736	Hydrophobic	Alkyl
		MET152[π .....Br]	4.781	Hydrophobic	Alkyl
		PHE164 [π .....Br]	4.753	Hydrophobic	Pi-Alkyl
		LYS58[C.....π]	5.085	Hydrophobic	Pi-Alkyl
		LEU98[C.....π]	5.019	Hydrophobic	Pi-Alkyl
Cabozantinib	-4.8	MET101[NH.....N]	2.882	Hydrogen Bond	Conventional Hydrogen Bond

		ILE32[CH.....π]	3.643	Hydrophobic	Pi-Sigma
		:UNL1:C27 - A:LEU85	3.970	Hydrophobic	Alkyl
		:UNL1:C27 - A:LEU98	4.096	Hydrophobic	Alkyl
		:UNL1:C27 - A:MET101	4.395	Hydrophobic	Alkyl
Crizotinib	-4.7	ASP105[NH.....N]	2.426	Hydrogen Bond	Conventional Hydrogen Bond
		ILE32[CH.....π]	3.885	Hydrophobic	Pi-Sigma
		MET152[CH.....π]	3.550	Hydrophobic	Pi-Sigma
		VAL40 [π .....C]	4.820	Hydrophobic	Alkyl
		ALA56 [π .....C]	3.544	Hydrophobic	Alkyl

4. CONCLUSIONS

A comprehensive analysis has been carried out on both the X-ray crystal structure and optimized structure of a series of halogenated aminopyridines. The molecular structure, Mulliken atomic charges, MEP, HOMO-LUMO energy gaps, and various other molecular properties of the optimized structure of halogenated aminopyridine derivatives have been investigated using DFT theory with the B3LYP/6-311++G(d,p) level basis set. The computed bond geometry is closely relatable to experimental values obtained from the crystallographic structures. The molecular orbital analysis indicates that the molecules look more stable and less reactive, with a large energy gap of 4.93 to 5.00 eV. The Hirshfeld surface analysis yields few important contacts such as N-H…N, C-H…Br, and C-H…Cl, respectively. The variation in void volume across the structures, by and large, is in a comparable range. The molecular docking analysis showed that all the investigated molecules exhibit much higher binding affinity in the range of -4.8 to -5.3 kcal/mol. Thus, all the molecules (M1–M5) are worthy of consideration as an efficient potent inhibitor for MET receptor.

5. ACKNOWLEDGMENTS

Rajni Kant expresses gratitude to the University of Jammu for providing financial assistance for authorised access to CSD.

6. REFERENCES

[1] Beer R H, Jimenez J, Drago R S. J. Org. Chem., 58, **1993,** 1746–1747,
doi : https://doi.org/10.1021/jo00059a024

[2] Nussbaumer S, Bonnabry P, Veuthey J L, Fleury-Souverain S. Talanta, 85, **2011,** 2265–2289, doi : https://doi.org/10.1016/j.talanta.2011.08.034

[3] De Clercq E. Biochem. Pharmacol., 85, **2013,** 727–744,
doi : https://doi.org/10.1016/j.bcp. 2012.12.011

[4] Beena and Rawat D S, Med. Res. Rev., 33, **2013,** 693–764,
doi : https://doi.org/10.1002/med. 21262

[5] Biamonte M A, Wanner J, Le Roch K G. Bioorg. Med. Chem. Lett., 23, **2013,** 2829–2843,
doi : https://doi.org/10.1016/j.bmcl.2013.03.067

[6] Hector R F. Clin. Tech. Small Anim. Pract., 20, **2005,** 240–249,
doi : https://doi.org/10.105 3/j.ctsap.2005.07.005

[7] Sung H, Ferlay J, Siegel R L, Laversanne M, Soerjomataram I, Jemal A, Bray F. CA: Cancer J. Clin., 71, **2021**, 209–249,
doi : https://doi.org/10.3322/caac.21660

[8] Moosavi F, Giovannetti E, Saso L, Firuzi O. Crit. Rev. Clin. Lab. Sci., 56, **2019,** 533–566,
doi : https://doi.org/10.1080/10408363.2019.1653821

[9] Mathieu L N, Larkins E, Akinboro O, Roy P, Amatya A K, Fiero M H, Mishra-Kalyani P S, Helms W S, Myers C E, Skinner A M, Aungst S, Jin R, Zhao H, Xia H, Zirkelbach J F, Bi Y, Li Y, Liu J, Grimstein M, Zhang X, Woods S, Reece K, Abukhdeir A M, Ghosh S, Philip R, Tang S, Goldberg K B, Pazdur R, Beaver J A, Singh H. Clin. Cancer Investig. J., 28, **2022,** 249–254, doi : https://doi.org/10.1158/1078-0432.CCR-21-1566

[10] Goubitz K, Sonneveld E J, Schenk H. Z. Kristallogr., 216, **2001,** 176–181,
doi : https://doi.org/10.1524/zkri.216.3.176.20326

[11] Pourayoubi M, Ghadimi S, Valmoozi A A E. Acta Cryst., E63, **2007,** o4631,
doi : https://doi.org/10.1107/S1600536807055328

[12] Adam M S S, Kindermann M K, Köckerling M, Heinicke J W. Eur. J. Org. Chem., **2009,** 4655–4665,
doi : https://doi.org/10.1002/ejoc.200900698

[13] Murthy P K, Rao R S, Suneetha V, Giri L, Suchetan P A. IUCrData., 2, **2017,** x170728,
doi : https://doi.org/10.1107/S2414314617007283

[14] Fun H K, Kia R, Maity A C, Maity S, Goswami, S. Acta Cryst., E65, **2009,** o97,
doi : https://doi.org/10.1107/S1600536808041366

[15] Frisch A. "Gaussian 09W Reference". Wallingford, USA, **2009,** p. 25.

[16] Mouada H., Lanez T., Zafar I. ROS scavenging, DNA binding and NADPH oxidase inhibition potential of N'-Ferrocenylmethyl-N'- phenylpropionohydrazide using cyclic voltammetry and molecular docking, *Journal of Organometallic Chemistry*. **2024**, https://doi.org/10.1016/j.jorganchem.2024.123026

[17] Yahiaoui A., Benyza N., Messai A., Lanez T., Lanez E. Voltametric and molecular docking investigations of ferrocenylmethylaniline and its N-acetylated derivative interacting with DNA, *Journal of Electrochemical Science and Engineering*. **2023**. https://doi.org/10.5599/jese.2061

[18] Mouada H., Lanez T., Zafar I, M.S. Afghan, N. Zegheb. N'-Ferrocenylmethyl-N'-phenylbenzohydrazide as a potential DNA binding compound: a combined experimental and computational study, *Journal of Coordination Chemistry*, **2023.** https://doi.org/10.1080/00958972.2023.2275247

[19] McKinnon J J, Spackman M A, Mitchell A S. Acta Cryst., B60, **2004,** 627-668,
doi : https://doi.org/10.1107/S0108768104020300

[20] Spackman M A, Jayatilaka D. CrystEngComm., 11, **2009,** 19-32,
doi : https://doi.org /10.1039/B818330A

[21] Spackman P R, Turner M J, McKinnon J J, Wolff S K, Grimwood D J, Jayatilaka D, Spackman M A. J. Appl. Crystallogr., 54, **2021,** 1006-1011,
doi : https://doi.org/10.1107/S160 0576721002910

[22] Wolff S K, Grimwood D J, McKinnon J J, Jayatilaka D, Spackamn M A. “Crystal Explorer 3.0”. University of Western Australia, Perth, **2007**.

[23] Spackman M A, McKinnon J J. CrystEngComm., 4(66), **2021,** 378–392,

doi : https://doi.org/10.1039/b203191b

[24] McKinnon J J, Mitchell A S, Spackman M A. Chem. Eur. J., **1998,** 2136-2141,

doi : https://doi.org/10.1002/(SICI)1521-3765(19981102)4:11<2136::AID-CHEM2136>3.0.CO;2-G

[25] Turner M J, McKinnon J J, Jayatilaka D, Spackman M A. CrystEngComm., 13(6), **2011,** 1804-1813,

doi : https://doi.org/10.1039/C0CE00683A

[26] Kargar H, Fallah-Mehrjardi M, Behjatmanesh-Ardakani R, Munawar K S, Ashfaq M, Tahir M N. J. Mol. Struct., 1241, **2021,** 130653,

doi : https://doi.org/10.1016/j.molstruc.2021.130653

[27] Kargar H, Fallah-Mehrjardi M, Behjatmanesh-Ardakani R, Tahir M N, Ashfaq M, Munawar K S. J. Coord. Chem., 74, **2021,** 2682,

doi : https://doi.org/10.1080/00958 972.2021.1972984

[28] Kargar H, Fallah-Mehrjardi M, Behjatmanesh-Ardakani R, Munawar K. S, Ashfaq M, Tahir M N. J. Mol. Struct., 1250, **2022,** 131691,

doi : https://doi.org/10.1016/j.molstruc. 2021.131691

[29] Morris G M, Huey R, Lindstrom W, Sanner M F, Belew R K, Goodsell D S, Olson A J. J. Comput. Chem., 30, **2009,** 2785-2791,

doi : http://doi.org/10.1002/jcc.21256.

[30] www.rcsb.org/pdb

[31] Dassault Systemes BIOVIA, [Discovery Studio 4.1 Visualizer], San Diego: Dassault Systemes, **2014.**

[32] Fukui K, Yonezawa T, Shingu H. J. Chem. Phys., 20, **1952,** 722-725,

doi : https://doi.org/10.1063/1.1700523

[33] Lanez E., Bechki L., Lanez T. Ferrocenylmethylnucleobases: Synthesis, DFT

calculations, electrochemical and spectroscopic characterization, *Chemistry & Chemical Technology*, **2020** 14(2), 146-153, https://doi.org/10.23939/chcht14.02.146

[34] Ruiz-Morales Y. J. Phys. Chem. A., 106, **2002,** 11283-11308,

doi : https://doi.org/10.1021/jp021 152e

[35] Seth S K. Acta Cryst., E74, **2018,** 600-606,

doi : https://doi.org/10.1107/S2056989018003857